Electronic Structure and Triplet-Triplet Energy Transfer in Artificial Photosynthetic Antennas

Marely E. Tejeda-Ferrari, Chelsea L. Brown, Gabriela C. C. C. Coutinho, Ghabriel A. Gomes De Sa, Julio L. Palma, Manuel J. Llansola-Portoles, Gerdenis Kodis, Vladimiro Mujica, Junming Ho, Devens Gust, et al.

Electronic Structure and Triplet-Triplet Energy Transfer in Artificial Photosynthetic Antennas

Marely E. Tejeda-Ferrari[1], Chelsea L. Brown[1], Gabriela C. C. C. Coutinho[1], Ghabriel A. Gomes de Sá[1], Julio L. Palma[2], Manuel J. Llansola-Portoles[3], Gerdenis Kodis[1], Vladimiro Mujica[1], Junming Ho*[4], Devens Gust*[1], Thomas A. Moore*[1], Ana L. Moore[1]*

[1]. School of Molecular Sciences, Arizona State University, Tempe, AZ 85287, USA, [2]. Department of Chemistry, The Pennsylvania State University, Fayette, The Eberly Campus, Lemont Furnace, PA 15456, USA, [3]. Institute for Integrative Biology of the Cell (I2BC), CEA, CNRS, Université Paris-Saclay, F-91198, Gif-sur-Yvette cedex, France, [4]. School of Chemistry, University of New South Wales, Sydney, NSW 2052, Australia.

*Corresponding authors e-mail: junming.ho@unsw.edu.au (Junming Ho) gust@asu.edu (Devens Gust), tmoore@asu.edu (Thomas A. Moore), amoore@asu.edu (Ana L. Moore)

ABSTRACT

Three Pd(II) phthalocyanine–carotenoid dyads featuring chromophores linked by amide bonds were prepared in order to investigate the rate of triplet-triplet (T-T) energy transfer from the tetrapyrrole to the covalently attached carotenoid as a function of the number of conjugated double bonds in the carotenoid. Carotenoids having 9, 10 and 11 conjugated double bonds were studied. Transient absorption measurements show that intersystem crossing in the Pd(II) phthalocyanine takes place in 10 ps in each case and that T-T energy transfer occurs in 126 ps, 81 ps and 132 ps in the dyads bearing 9, 10 and 11 double bond carotenoids, respectively. To identify the origin of this variation in T-T energy transfer rates, density functional theory (DFT) was used to calculate the T-T electronic coupling in the three dyads. According to the calculations, the primary reason for the observed T-T energy transfer trend is larger T-T electronic coupling between the tetrapyrrole and the 10-double bond carotenoid. A methyl group adjacent to the amide linker that connects the Pd(II) phthalocyanine and the carotenoid in the 9 and 11-double bond carotenoids is absent in the 10-double bond carotenoid, and this difference alters its electronic structure to increase the coupling.

INTRODUCTION

In photosynthetic organisms, solar energy is collected by light-harvesting complexes and the excitation energy is transferred to reaction centers, where it is converted into electrochemical potential by charge separation (1). The key light-harvesting molecules in these complexes are chlorophylls (tetrapyrroles), but carotenoids are also present as accessory antenna pigments. Carotenoids harvest light in the blue/green region of the visible spectrum where chlorophylls have low absorptivity. Additionally, because of the large structural variability of carotenoids their spectral properties can be tuned to optimize the fitness of an organism for a particular ecological niche (2-4).

In photosynthesis carotenoids not only act as antenna molecules, but also play a central role in photoregulation and photoprotection (5-7). When a photosynthetic organism is exposed to high light conditions, carotenoids photoregulate by dissipating excess singlet excitation energy in the form of heat through non-photochemical quenching (NPQ) by at least three types of mechanisms (5, 7-10). Photoprotection by carotenoids is another vital process that operates in all photosynthetic organisms and has been studied for decades. When a singlet excited state is formed in a chlorophyll, it can undergo intersystem crossing (ISC) to the triplet state, which is a potent sensitizer of singlet oxygen. Singlet oxygen is a reactive oxygen species and is one of the most dangerous chemical species for cellular components (6, 11-13). It has been determined that when the chlorophyll and carotenoid interchromophore distance is very short (essentially van der Waals contact), triplet-triplet (T-T) energy transfer from the chlorophyll to the carotenoid takes place. This process reduces the lifetime of the chlorophyll triplet state by many orders of magnitude, rendering it kinetically incompetent to sensitize singlet oxygen (14,

15). The energy of the triplet excited state of the carotenoids lies below that of singlet oxygen (0.97 eV) and hence it cannot sensitize singlet oxygen, and decays harmlessly to the ground state (12, 6). It is well-known that in purple bacteria bacteriochlorophyll-to-carotenoid T-T energy transfer occurs on the nanosecond time scale (20-200 ns) (16). This process is relatively slow compared to that in the light-harvesting complex II (LHCII) of higher plants, where it has not been precisely measured but it is known to be much faster than the singlet chlorophyll lifetime of ~3 ns (12). Such fast T-T transfer has not only been measured in plant LHCII, but also in the peridinin-chlorophyll protein (17) and fucoxanthin-chlorophyll protein of algae, (18, 19) suggesting that it is conserved in oxygenic photosynthesis. It has been postulated that such ultrafast quenching of the triplet state of chlorophylls is an example of a molecular photoprotective adaptation that took place during the evolution of oxygenic photosynthesis (20).

It is important to understand the photoprotective mechanisms extant in nature in order to adapt them to improve the functionality and lifespan of reengineered photosynthesis and other artificial photosynthetic systems. Indeed, to sustainably meet human needs for food, fuel and biomass photosynthesis could/must be reengineered to produce up to a ca. 10-fold increase in biomass yield, which will result in a concomitant increase in O_2 production. As mentioned above, studies of photoprotection in bacteria and higher plants suggest that evolutionary processes provide levels of photoprotection in response to ambient O_2 levels. Although a sudden large increase in O_2 production in a reengineered photosynthetic plant would not be expected to increase ambient O_2 levels, it could transiently increase local levels in the thylakoid membranes close to the oxygen-evolving complex and nearby chlorophylls resulting in photodamage due to singlet oxygen sensitization. To avoid this possibility, a much higher level of photoprotection could be initially engineered into the improved photosynthetic systems. This requires an atomic

level understanding of the parameters controlling tetrapyrrole-carotenoid interactions. Importantly, these interactions control light harvesting, photoregulation and photoprotection and the factors controlling these three separate functions must be identified in order to resolve the apparent paradox that the same or similar carotenoids can provide both light harvesting and photoregulation, which are contradictory functions (21-23).

To contribute to a fundamental understanding of T-T energy transfer mechanisms relevant to photosynthesis, we have designed and prepared a series of bio-inspired dyads consisting of carotenoids of different conjugation lengths (9, 10, and 11 double bonds) and a phthalocyanine linked by an amide group. The amide was chosen due to its proven stability and because it provides good electronic coupling between carotenoids and phthalocyanines (5, 8, 9, 24). The phthalocyanine has been metallated with palladium in order to use the heavy atom effect to increase the rate of ISC (25). Because the two chromophores absorb in different regions of the visible spectrum, selective excitation of the phthalocyanine moiety followed by fast ISC to form its triplet state in high yield is possible. Thus, measurement of the rate of the subsequent T-T energy transfer to the carotenoid is facilitated.

MATERIALS AND METHODS

General analytical: Steady state UV-visible spectra were obtained with a Shimadzu UV-2559 UV-visible spectrophotometer. Mass spectrometry was performed with a Voyager DE-STR matrix-assisted laser desorption/ionization time-of-flight spectrometer (MALDI-TOF), equipped with a 60 Hz laser, using (1E, 3E)-1,4-diphenylbuta-1,3-diene (DPB) as a matrix. The reported mass is that of the most abundant isotope observed. The ^{1}H-NMR spectra were taken

on a Varian spectrometer at 400 MHz. Samples were prepared using deuterated solvents containing 0.03% tetramethylsilane as an internal standard.

Time resolved fluorescence: Fluorescence decay measurements were performed by the time-correlated single-photon-counting method. The excitation source was a fiber supercontinuum laser based on a passive mode locked fiber laser and a high-nonlinearity photonic crystal fiber supercontinuum generator (Fianium SC450). The laser provides 6-ps pulses at a repetition rate variable between 0.1 and 40 MHz. The laser output was sent through an acousto-optical tunable filter (Fianium AOTF) to obtain excitation pulses at desired wavelengths in the ca. 450-900 nm region. Fluorescence emission was detected at the magic angle using a double grating monochromator (Jobin Yvon Gemini-180) and a microchannel plate photomultiplier tube (Hamamatsu R3809U-50). The instrument response function was 35-55 ps. The spectrometer was controlled by software based on the LabView programming language and data acquisition was done using a single photon counting card (Becker-Hickl, SPC-830). The data analysis was carried out using locally written software (ASUFIT) developed in the MATLAB environment (Mathworks Inc.). Data were fitted as a sum of exponential decays which were reconvoluted with the appropriate instrument response function. Goodness of fit was established by examination of residuals and the reduced χ^2 value.

Transient absorption: Femtosecond to nanosecond transient absorption measurements were acquired with a 1 kilohertz pulsed laser source and a pump-probe optical setup. Laser pulses at 800 nm (c.a. 100 fs) were generated from an amplified, mode-locked titanium sapphire kilohertz laser system (Millennia/Tsunami/Spitfire, Spectra Physics). Part of the laser pulse energy was sent through an optical delay line and focused onto a 3 mm sapphire plate to generate a white

light continuum for the probe beam. The remainder of the pulse energy was used to pump an optical parametric amplifier (Spectra Physics) to generate excitation pulses at 700 nm, which were selected using a mechanical chopper. The white light probe beam was compressed by prism pairs (CVI) before passing through the sample. The polarization of the pump beam was set to the magic angle (54.7°) relative to the probe beam and its energy was adjusted to 200 nJ using a continuously variable neutral density filter. The beams were focused in a 2 mm path-length quartz cuvette to a ~400 μm diameter spot. The white light probe was dispersed by a spectrograph (300 line grating) onto a charge-coupled device (CCD) camera (DU420, Andor Tech.). The final spectral resolution was about 2.3 nm for over a nearly 300 nm spectral region. The instrument response function was ca. 100 fs. The decay-associated spectra (DAS) were obtained by fitting globally the transient absorption kinetic traces over a selected wavelength region simultaneously as described by equation (1) (parallel kinetic model) (26), where $\Delta A(\lambda,t)$

$$\Delta A(\lambda,t) = \sum_{i=1}^{n} A_i(\lambda)\exp\left(-t/\tau_i\right) \qquad (1)$$

is the observed absorption change at a given wavelength at time delay t and n is the number of kinetic components used in the fitting. A plot of $A_i(\lambda)$ versus wavelength is called a Decay Associated Spectra (DAS) and represents the amplitude spectrum of the ith kinetic component, which has a lifetime of τ_i. Random errors associated with the reported lifetimes obtained from transient absorption measurements were typically ≤ 5%.

Synthesis: The 4-hexanamidophthalonitrile was synthesized following a previously published method (5). The carotenoid esters, methyl 8'-apo-β-caroten-8'-oate (9 double bonds), methyl 6'-apo-β-caroten-6'-oate (10 double bonds), and methyl 4'-apo-β-caroten-4'-oate (11 double

bonds), were prepared as described before (27, 28) and the corresponding acids were obtained by base promoted hydrolysis.

Pd(II) 8,11,15,18,22,25-hexabutoxy-2-hexanamidophthalocyanine (Pc): Portions of 4-hexanamidophthalonitrile (456 mg, 1.89 mmol), 3,6-dibutoxyphthalonitrile (1.50 g, 5.67 mmol), and $PdCl_2$ (603 mg, 3.40 mmol) were dissolved in 30 mL of butanol, heated to 45 °C, and flushed with argon for 15 min. A portion of 1,8-diazabicyclo[5.4.0]undec-7-ene (DBU, 3.39 ml) was added and the solution was heated to 118 °C. The reflux was kept overnight under a blanket of argon. The green mixture was cooled to room temperature and 100 mL of a water/chloroform mixture (1:1) was added. The organic layer was extracted, dried over Na_2SO_4, and filtered. The solvent was concentrated by rotary evaporation. The product was purified by column chromatography (silica gel, 1% MeOH/10% ethyl acetate/$CHCl_3$). Pd(II) 8,11,15,18,22,25-hexabutoxy-2-hexanamidophthalocyanine was obtained in 1.05 % yield (23 mg). ^{1}H-NMR δ ppm (20% Pyridine-d/$CDCl_3$): 1.09 (t, J = 7.4, 7.4 Hz, 3H), 1.27 (m, 18H), 1.70 (m, 4H), 2.24 (q, 2H), 2.39 (t, J = 7.5, 7.5 Hz, 2H), 3.20-5.20 (m, 36H), 6.85 (d, J = 8.7 Hz, 1H), 7.13 (d, J = 8.8 Hz, 1H), 7.38 (d, J = 9.6 Hz, 1H), 7.52 (d, J = 9.3 Hz, 1H), 7.64 (m, 2H), 8.31 (d, J = 7.8 Hz, 1H), 9.26 (d, J = 7.9 Hz, 1H), 10.03 (s, 1H), 10.84 (s, 1H). MALDI-TOF: m/z obsd. 1163.46 calc. for $C_{62}H_{75}N_9O_7Pd$ 1163.48. UV/vis λ_{max} (95% $CHCl_3$/5% MeOH): 327, 647, and 721 nm.

Pd(II) 2-amino-8,11,15,18,22,25-hexabutoxyphthalocyanine: The hexanamido-phthalocyanine obtained in the above reaction (20.4 mg, 17.6 μmol) was dissolved in 10 mL of tetrahydrofuran (THF) and 5 mL of a saturated methanolic solution of KOH. The solution was heated to 65°C and stirred overnight. The reaction mixture was diluted with chloroform and washed with water (three times). The organic layer was dried over Na_2SO_4 and filtered, and the solvent was removed by rotary evaporation. The desired Pd(II) 2-amino-8,11,15,18,22,25-hexabutoxyphthalocyanine (18.5 mg) was obtained in 99 % yield. MALDI-TOF: m/z obsd.

1065.32 calc. for $C_{56}H_{65}N_9O_6Pd$ 1065.41. UV/vis λ_{max} (95% $CHCl_3$/5% MeOH): 324, 647, and 721 nm.

Dyad-9: The 8'-apo-β-caroten-8'-oic acid (28.5 mg, 65.7 μmol) and Pd(II) 2-amino-8,11,15,18,22,25-hexabutoxyphthalocyanine (35 mg, 32.9 μmol) were dissolved in 45 mL of dry chloroform. While under argon, 1-ethyl-3-(3-dimethylaminopropyl)carbodiimide (EDCI, 68.9 mg, 0.36 mmol) and 4-dimethylaminopyridine (224 mg, 1.83 mmol) were added. The reaction was stirred overnight at room temperature under a blanket of argon. The solvent was removed by rotary evaporation and the product was purified by column chromatography (silica, 2% MeOH/dichloromethane). The product was then purified by two preparative TLCs, the first in 1% MeOH/5% ethyl acetate/chloroform and the second in 2% MeOH/dichloromethane. **Dyad-9** (5.7 mg) was obtained in 12 % yield. ^{1}H-NMR δ ppm (5% pyridine-d/$CDCl_3$): 0.68 (m, 6H), 0.88 (m, 18H), 1.02 (m, 4H), 1.10 (m, 6H), 1.18 (s, 2H), 1.65 (m, 15H), 1.98 (m, 6H), 2.30 (m, 12H), 4.98 (m, 12H), 6.21-6.85 (m, 11H), 7.11 (d, J = 9.0 Hz, 1H), 7.37 (m, 1H), 7.51 (m, 1H), 7.71 (m, 1H), 8.04 (d, J = 8.1 Hz, 1H), 8.45 (d, J = 9.3 Hz, 1H), 9.22 (s, 2H), 9.44 (s, 1H), 9.62 (s, 1H), 10.14 (s, 1H). MALDI-TOF: m/z obsd. 1479.98 calc. for $C_{86}H_{103}N_9O_7Pd$ 1479.70. UV/vis λ_{max} (95% $CHCl_3$/5% MeOH): 330, 454, 648, and 722 nm.

Dyad-10: It was prepared by the same procedure described for **dyad-9** except using 6'-apo-β-caroten-6'-oic acid (6.8 mg, 18% yield). ^{1}H-NMR δ ppm (5% pyridine-d/$CDCl_3$): 0.68 (m, 6H), 0.88 (m, 18H), 1.02 (m, 4H), 1.10 (m, 6H), 1.18 (s, 2H),), 1.65 (m, 15H), 1.98 (m, 6H), 2.30 (m, 12H), 4.98 (m, 12H), 6.05-6.87 (m, 13H), 7.07 (d, J = 12.1 Hz, 1H), 7.50 (m, 1H), 7.60 (m, 1H), 7.71 (m, 1H), 8.04 (d, J = 8.2 Hz, 1H). 8.38 (s, 1H), 9.22 (s, 2H), 9.67 (s, 1H), 9.74 (s, 1H), 9.95 (s, 1H). MALDI-TOF: m/z obsd. 1505.70 calc. for $C_{88}H_{105}N_9O_7Pd$ 1505.72. UV/vis λ_{max} (95% $CHCl_3$/5% MeOH): 327, 470, 650, and 725 nm.

Dyad-11: It was prepared by the same procedure described for **dyad-9** except using 4'-apo-β-caroten-4'-oic acid (8.1 mg, 9.8% yield). ^{1}H-NMR δ ppm (5% pyridine-d/$CDCl_3$): 0.68 (m,

6H), 0.88 (m, 18H), 1.02 (m, 4H), 1.10 (m, 6H), 1.18 (s, 2H), 1.65 (m, 15H), 1.98 (m, 6H), 2.30 (m, 12H), 4.98 (m, 12H), 6.05-6.88 (m, 15H), 7.07 (d, J = 10.4 HZ, 1H), 7.46 (d, 1H), 7.52 (m, 1H), 7.60 (m, 2H), 8.38 (s, 1H), 8.52 (d, J = 8.1 Hz, 1H), 8.93 (s, 1H), 9.23 (d, J = 7.9 Hz, 1H), 9.48 (s, 1H), 9.55 (s, 1H). MALDI-TOF: m/z obsd. 1545.83 calc. for $C_{91}H_{109}N_9O_7Pd$ 1545.75. UV/vis λ_{max} (95% $CHCl_3$/5% MeOH): 330, 482, 649, and 723 nm.

Computational details: All electronic structure calculations were carried out using the Gaussian 09 (29) and Q-CHEM programs (30). The geometries of the dyads were optimized using the dispersion corrected (B3LYP+GD3BJ) (31, 32) and with 6-31G(d) basis set specified for all atoms, except Pd, where the lanl2dz basis set was used. The triplet-triplet coupling was computed using the fragment excitation difference (FED) (33) method implemented in Q-CHEM, (30) and these were evaluated at the TD-B3LYP/6-31G(d) level (employing the Tamm-Dancoff approximation). The expression for the FED method is shown in equation (2).

$$V = \frac{(E_2 - E_1)|\Delta x_{12}|}{\sqrt{(\Delta x_{11} - \Delta x_{22}) + 4\Delta x_{12}^2}} \qquad (2)$$

$\Delta E = (E_2 - E_1)$ is the difference in energies of the porphyrin and the carotenoid triplet states defined by (Por(S0)-Car(T1) and Por(T1)-Car(S0)); the $|\Delta x_{12}|$ term measures the extent of delocalization of the excited states calculated by subtracting the appropriated electron densities on the acceptor and donor fragments (34). The boundary between the donor and acceptor fragments is defined to be at the C–N amide bond. Ideally, the energies should be evaluated on Por(T1)-Car(S0) geometry, i.e., after ISC. For **dyad-9'**, we found that the RMSD between the Por(T1)-Car(S0) and Por(S0)-Car(S0) optimized geometries is 0.06 Å. Accordingly in the present work, we made an approximation by carrying out FED calculations on the ground state geometries, Por(S0)-Car(S0) (See Fig. S2 in Supplementary Materials).

RESULTS

Synthesis

The synthesis of the Pd(II) phthalocyanine (**Pc**) was achieved by the condensation reaction of 4-hexanamidophthalonitrile (5) and 3,6-dibutoxyphthalonitrile, in the presence of $PdCl_2$. Those reagents were heated to reflux in butanol in the presence of 1,8-diazabicyclo[5.4.0]undec-7-ene (DBU) to yield the statistical mixture of phthalocyanines. Thin layer chromatography (TLC) of the reaction crude showed four main products: the less polar Pd(II) 1,4,8,11,15,18,22,25-octabutoxyphthalocyanine side product, the desired phthalocyanine, **Pc**, the more polar Pd(II) 15,18,22,25-tetrabutoxy-2,9-dihexanamidophthalocyanine and its regioisomeric side products, and the very polar Pd(II) 22,25-dibutoxy-2,9,16-trihexanamidophthalocyanine and its regioisomeric side products. The polarity differences between the products allowed separation using silica column chromatography to yield **Pc** (1% yield). The amide group of **Pc** was hydrolyzed under basic conditions to form Pd(II) 2-amino-8,11,15,18,22,25-hexabutoxyphthalocyanine (99% yield). To prepare the dyads, the carboxylic acid carotenoids of various double bond conjugation lengths (9, 10, and 11 double bonds) were synthesized following a previously published procedure (27). The coupling of the carboxylic acid carotenoids to the aminophthalocyanine was done in chloroform using 1-ethyl-3-(3-dimethylaminopropyl)carbodiimide hydrochloride (EDCI) as the coupling reagent with 4-dimethylaminopyridine (DMAP) as the base. Each dyad was purified using silica column chromatography and multiple preparative TLCs to give **dyad-9** in 12% yield, **dyad-10** in 18% yield, and **dyad-11** in 10% yield (Fig. 1).

<Figure 1>

Steady-state absorption

Fig. 2 shows the absorption spectra of **dyad-9**, **dyad-10**, **dyad-11**, and the reference **Pc** in toluene. The absorption band with maximum around ~320 nm corresponds to the Soret band of **Pc** and the bands with maxima at ~640 nm and 720 nm correspond to the **Pc** Q bands. The broad absorption bands between ~400 and 550 nm are associated primarily with the carotenoid absorption and, as expected, shift to the red with increasing conjugation length. The spectra of the individual dyes are minimally perturbed by forming the dyads.

<Figure 2>

Time resolved fluorescence

Time-resolved fluorescence measurements for **dyad-10** show fast (~10 ps) decay of the **Pc** singlet excited state (see Supplementary Materials, Fig. S1); similar results were obtained for the other dyads and model **Pc** (not shown). The decay of the phthalocyanine first excited singlet state on this short time scale is ascribed mainly to formation of the corresponding phthalocyanine triplet state, as shown by the transient absorption results discussed below.

Transient absorption spectroscopy

In order to further elucidate the fate of the excited singlet state of the Pc in the dyads, transient absorption measurements were performed for the three dyads and **Pc**. As mentioned before, carotenoids have no absorption in the 700 nm region and above. Therefore it is possible to selectively excite just the phthalocyanine moiety of a dyad at 700 nm. Global analysis of the transient absorption data obtained upon 700 nm excitation of **Pc** and for the three dyads dissolved in toluene gave the decay-associated spectra (DAS) shown in Fig. 3. For **Pc**, four

DAS with time constants of 0.5 ps, 11 ps, 90 ps, and a non-decaying (on the 1 ns time scale) component are associated with the decay of the **Pc** excited state. The 11 ps DAS shows the decay of the **Pc** singlet excited state forming ^{3}**Pc** (ISC) with appearance of the triplet excited state induced absorption at around 600 nm. The 0.5 ps DAS and 90 ps DAS are associated with the relaxation/solvation of the **Pc** singlet and triplet excited states, respectively. The 0.5 ps DAS shows the characteristic derivative like feature (positive amplitude on the red side of the bleaching band and negative amplitude on the blue side) corresponding to the red shift and increase of the Q band bleaching at ~710 nm due to relaxation/solvation. The non-decaying DAS is associated with ^{3}**Pc**, and shows the characteristic induced absorption at around 600 nm and Q band bleaching at ~710 nm.

<Figure 3>

Global analysis of the transient absorption data for **dyad-9** gave four DAS with time constants of 2 ps, 10 ps, 126 ps, and a non-decaying component (Fig. 3 b). The 2 ps component in this and the other dyads is associated with the relaxation/solvation of the **Pc** singlet excited state. The 10 ps DAS is associated with the decay of the **Pc** singlet-excited state to form ^{3}**Pc** (ISC), because it shows the formation/rise (negative amplitude) of the induced absorption at around 625 nm. The 126 ps DAS corresponds to T-T energy transfer between ^{3}**Pc** and the carotenoid to yield triplet carotenoid (^{3}**Car**), and it shows the rise of the induced absorption characteristic of the ^{3}**Car** at around 530 nm and simultaneous decay of the ground state bleaching at ~710 nm associated with ^{3}**Pc** returning to the ground state. The non-decaying DAS is due to ^{3}**Car**, which eventually decays to the ground state. Note that this DAS also shows a bleaching band at ~710 nm associated with the **Pc**. This phenomenon is a characteristic of

strongly coupled carotenoid-tetrapyrrole systems and its presence has been known for a long time, but its origin is not well understood (35, 36). These results indicate that the T-T energy transfer from the **^{3}Pc** to the triplet excited state of the 9-double bond carotenoid in **dyad-9** occurs with a time constant of 126 ps.

For **dyad-10** the global analysis of the transient absorption data gave four DAS with time constants of 2 ps, 10 ps, 81 ps, and a non-decaying component (Fig. 3 c). Similar to **dyad-9**, the 10 ps DAS is associated with the formation of **^{3}Pc** (ISC). The 81 ps DAS in **dyad-10** corresponds to the T-T energy transfer from **^{3}Pc** to yield **^{3}Car**, again because the characteristic **^{3}Car** induced absorption at around 550 nm grows in (negative amplitude), while simultaneously the decay of the ground state bleaching of **^{3}Pc** at 710 nm is observed. These results indicate that the T-T energy transfer from the **^{3}Pc** to the 10-double bond carotenoid triplet in **dyad-10** occurs in 81 ps, which is faster than for **dyad-9**. As before, the non-decaying DAS is associated with the decay of **^{3}Car**. In **dyad-11** the picture is similar to that of **dyad-9** with DAS of 2ps, 10 ps, 132 ps, and a non-decaying component (Fig. 3 d). The 132 ps DAS in **dyad-11** corresponds to T-T energy transfer from **^{3}Pc** to yield **^{3}Car**.

<Figure 4>

Theoretical calculations

Theoretical computations were performed in an attempt to determine the structural basis for the trend in the experimental rates of T-T energy transfer from the phthalocyanine to the appended carotenoids in the dyads. For purposes of computation, models of **dyad-9**, **dyad-10** and **dyad-11**, indicated as **dyad-9'**, **dyad-10'** and **dyad-11'**, were generated. Note that in the

computational models the butoxy groups of the phthalocyanine moiety were replaced by methoxy groups. Values for the electronic coupling (|V|) promoting T-T energy transfer were obtained using the fragment excitation difference (FED) scheme (37) (see Computational details, above) were determined to be 11.5, 13.7 and 8.7 cm^{-1} for **dyad-9'**, **dyad-10'** and **dyad-11'**, respectively. The values of |V| are qualitatively consistent with the trend of the experimental T-T energy transfer time constants observed for **dyad-9**, **dyad-10** and **dyad-11** of 129, 80 and 130 ps.

The reason for the enhanced coupling in **dyad-10** relative to the other dyads is not readily apparent from a cursory examination of the structures. However, one structural difference involves the absence of a methyl group on the carbon of the double bond nearest the amide linkage. This absence is a consequence of the reagent chosen in the Wittig reaction to prepare this carotenoid. To better understand the experimental trend in T-T-energy transfer, we considered other computational models, one of which lacks all the methyl groups on the polyene chain (**dyad-9''**, **dyad-10''** and **dyad-11'')**. Additionally, models of **dyad-9'** and **dyad-11'**, in which only the methyl group adjacent the amide linking group was replaced by a hydrogen atom were evaluated (**dyad-9'''** and **dyad-11'''**). The structures of all the computational models are shown in Fig. 5 and the results are summarized in Table 1. The individual components of the FED coupling expression (see Computational details, above) are summarized in the Supplementary Materials, Tables S1–3.

<Figure 5>

Interestingly, the computed T-T energy transfer couplings for the dyads containing non-methylated carotenoids on the polyene backbone (**dyad-9''**, **dyad-10''** and **dyad-11''**) decrease

monotonically as the carotenoid chain length increases. Analysis of the individual contributions to the electronic coupling (see Table S2, Supplementary Materials) indicates that longer conjugated carotenoid chains lead to a larger ΔE (the carotenoid triplet becomes lower in energy), and the resulting triplet excited states also become more localized on the polyene (smaller $|\Delta x_{12}|$). As shown in equation (2), the coupling depends strongly on the two effects (ΔE and $|\Delta x_{12}|$), which appears to be acting in opposite directions in these systems (the denominator has a value around 4 for all the dyads – see Table S2). Comparison with **dyads-9'**, **dyad-10'** and **dyad-11'** (see Table S1, Supplementary Materials) further indicates that the non-methylated carotenoids lead to an increased energy difference between the donor-acceptor triplet states (larger ΔE) and that appears to be the origin of the larger coupling values for these model dyads. In addition, the optimized geometries of **dyad-9''**, **dyad-10''** and **dyad-11''** display carotenoid conformations that are linearly extended, whilst the carotenoids in **dyads-9'**, **dyad-10'** and **dyad-11'** are significantly curved (see Figure 6) (38). To investigate the effect of this geometrical difference, T-T couplings were computed on *partially optimized* geometries of **dyad-9''**, **dyad-10''** and **dyad-11''** where the carotenoid chain is constrained to the geometries in **dyads-9'**, **dyad-10'** and **dyad-11'**. As shown in Table 1 (see values in parentheses), the curvature in the carotenoid chain attenuates the T-T coupling. This suggests that the origin of the trend in T-T coupling for **dyads-9'**, **dyad-10'** and **dyad-11'** may be due to a geometrical effect induced by the presence of methyl groups on the carotenoid backbone.

<Figure 6>

To examine the effect of the methyl group adjacent the amide linkage, we considered the computational models **dyad-9'''**, **dyad-10'** and **dyad-11'''** where a hydrogen atom was

substituted for a methyl group in the case of **dyad-9'''** and **dyad-11'''** (the methyl group is not present in this position in **dyad-10'**). The results clearly indicate that absence of the adjacent methyl group in **dyad-9'''** and **dyad-11'''** increases the magnitude of the T-T energy transfer coupling compared with **dyad-9'** and **dyad-11'** (see Table 1). The origin of this trend is in the $|\Delta x_{12}|$ term (see Table S1 and S3, Supplementary Materials). The similarity in T-T transfer coupling in **dyad-9''**, **dyad-10''** and **dyad-11''** indicates that the adjacent methyl group exerts a particularly strong influence.

<Table 1>

In summary, these calculations suggest that the presence of a methyl group adjacent to the amide linkage leads to triplet states that are more localized and consequently have smaller coupling values as observed in **dyad-9'** and **dyad-11'**. In addition, there appears to be a geometrical effect induced by the presence of methyl groups on the carotenoid backbone.

DISCUSSION

The experimental data show that for all three dyads, the phthalocyanine singlet state formed upon excitation rapidly decays by ISC to give the phthalocyanine triplet and by other pathways. The phthalocyanine triplet then decays by T-T transfer to produce the carotenoid triplet state. The time constants for the T-T transfer are 126 ps, 81 ps and 132 ps for **dyad-9**, **dyad-10** and **dyad-11**, respectively (Fig. 4). If we make the reasonable assumption that increasing the carotenoid chain length increases the thermodynamic driving force for T-T transfer and concurrently the spectral overlap, (27) we would expect that the rate of T-T transfer would increase as the number of double bonds in the carotenoid increases. Clearly, this is not the case.

In addition to thermodynamic effects, electronic coupling also plays an important role in determining T-T transfer rates. We therefore undertook theoretical calculations in order to determine values for carotenoid-phthalocyanine electronic coupling for each dyad, and for some relevant computational structures. First-principle DFT calculations show that the electronic coupling promoting T-T energy transfer for **dyad-10** is stronger than those for **dyad-9** and **dyad-11**, which is in agreement with the kinetic measurements. The calculations indicate that carotenoids having a methyl group adjacent to the amide linkage (as in **dyad-9** and **dyad-11)** lead to triplet states that are more localized and consequently have smaller coupling values than those of carotenoids lacking such methyl groups, as in **dyad-10**. Our calculations also suggest that conformational changes (a slight S-shape in the carotenoid) due to the presence of the methyl groups along the carotenoid backbone must also be considered a factor in increasing the coupling in **dyad-10** over that in **9** and **ll**. We therefore associate the change in coupling due to methyl groups acting in two ways. There is an intrinsic effect of the methyl group near the amide bond on the electronic structure of the triplet state, which gives rise to the observed changes in T-T transfer rates. There is also a change in the electronic structure of the triplet state due to a conformational change driven by the methyl groups along the carotenoid backbone, which increases the T-T transfer rate in **dyad-10**.

CONCLUSIONS

In this work we directly determined T-T transfer rates in model systems mimicking oxygenic photosynthesis and demonstrated that T-T transfer rates are much faster than the natural ISC rate and tetrapyrrole singlet lifetime, which is a prerequisite for effective triplet state quenching of the tetrapyrrole and prevention of singlet oxygen sensitization. The experimental and theoretical

investigation of T-T transfer in a set of three carotenoid-phthalocyanine dyads shows that the transfer rate is a function of the electronic coupling via the linkage joining the carotenoid and phthalocyanine.

Relatively small changes in carotenoid structure near this linkage have discernable effects on T-T transfer rates. Because antenna function (S-S energy transfer), photoprotection (T-T energy transfer) and photoregulation (S-S energy transfer, electron transfer and excitonic coupling) (8) by carotenoids in artificial photosynthetic constructs and in photosynthesis are functions of the electronic coupling between the two chromophores, the results of this study suggest that a detailed understanding of the electronic coupling is an important design feature of artificial photosynthetic systems that incorporate carotenoid and tetrapyrrole chromophores. It is important to define structures in which those features of the electronic coupling that would favor the desired process, light harvesting or photoregulation, can be identified. Taken together, light harvesting and photoregulation make up an apparent energy wasting futile cycle. In fact, such cycles are known in metabolic pathways where they play a crucial role in regulating metabolic flux to maintain near constant ATP chemical potential in response to changing bioenergetic demands on the cell, (39) but they are not known to play such roles in the primary photophysics of photosynthesis.

ACKNOWLEDGMENTS: This research was supported by the U.S. Department of Energy, Office of Science, Office of Basic Energy Sciences, under Award DE-FG02-03ER15393. JH acknowledges the Australian Research Council for financial support (Grant No. DE160100807) and the Australian NCI and Intersect Australia Ltd for generous allocation of computational resources.

SUPPLEMENTARY MATERIALS

Figure S1, Table S1–S3 and the cartesian coordinates of the DFT optimized geometries can be found at DOI: 10.1562/2006-xxxxxx.s1.

REFERENCES

1. Blankenship, R. E. (2014) *Molecular mechanisms of photosynthesis* Wiley Blackwell, Oxford, UK, NJ, USA.

2. Polívka, T. and H. A. Frank (2010) Molecular factors controlling photosynthetic light harvesting by carotenoids. *Acc. Chem. Res.* **43**, 1125-1134.

3. Croce, R. and H. van Amerongen (2014) Natural strategies for photosynthetic light harvesting. *Nat. Chem. Biol.* **10**, 492-501.

4. Fuciman, M., G. Keşan, A. M. LaFountain, H. A. Frank and T. Polívka (2015) Tuning the spectroscopic properties of aryl carotenoids by slight changes in structure. *J. Phys. Chem. B* **119**, 1457-1467.

5. Berera, R., C. Herrero, I. H. M. van Stokkum, M. Vengris, G. Kodis, R. E. Palacios, H. van Amerongen, R. van Grondelle, D. Gust, T. A. Moore, A. L. Moore and J. T. M. Kennis (2006) A simple artificial light-harvesting dyad as a model for excess energy dissipation in oxygenic photosynthesis. *Proc. Natl. Acad. Sci. U. S. A.* **103**, 5343-5348.

6. Frank, H. A. and R. J. Cogdell (1996) Carotenoids in photosynthesis. *Photochem. Photobiol.* **63**, 257-264.

7. Holt, N. E., D. Zigmantas, L. Valkunas, X.-P. Li, K. K. Niyogi and G. R. Fleming (2005) Carotenoid cation formation and the regulation of photosynthetic light harvesting. *Science* **307**, 433-436.

8. Kloz, M., S. Pillai, G. Kodis, D. Gust, T. A. Moore, A. L. Moore, R. van Grondelle and J. T. M. Kennis (2011) Carotenoid photoprotection in artificial photosynthetic antennas. *J. Am. Chem. Soc.* **133**, 7007-7015.

9. Berera, R., I. H. M. van Stokkum, G. Kodis, A. E. Keirstead, S. Pillai, C. Herrero, R. E. Palacios, M. Vengris, R. van Grondelle, D. Gust, T. A. Moore, A. L. Moore and J. T. M. Kennis (2007) Energy transfer, excited-state deactivation, and exciplex formation in artificial carotenophthalocyanine light-harvesting antennas. *J. Phys. Chem. B* **111**, 6868-6877.

10. Staleva, H., J. Komenda, M. K. Shukla, V. Šlouf, R. Kaňa, T. Polívka and R. Sobotka (2015) Mechanism of photoprotection in the cyanobacterial ancestor of plant antenna proteins. *Nat. Chem. Biol.* **11**, 287-291.

11. Polívka, T. and V. Sundström (2004) Ultrafast dynamics of carotenoid excited states−from solution to natural and artificial systems. *Chem. Rev.* **104**, 2021-2072.

12. Gall, A., R. Berera, M. T. A. Alexandre, A. A. Pascal, L. Bordes, M. M. Mendes-Pinto, S. Andrianambinintsoa, K. V. Stoitchkova, A. Marin, L. Valkunas, P. Horton, J. T. M. Kennis, R. van Grondelle, A. Ruban and B. Robert (2011) Molecular adaptation of photoprotection: Triplet states in light-harvesting proteins. *Biophys. J.* **101**, 934-942.

13. Foote, C. S. (1976) Photosensitized oxidation and singlet-oxygen: Consequences in biological systems. In *Free radicals in biology*, Vol. 2. (Edited by W. A. Pryor). Academic Press, New York.

14. Monger, T. G., R. J. Cogdell and W. W. Parson (1976) Triplet states of bacteriochlorophyll and carotenoids in chromatophores of photosynthetic bacteria. *Biochim. Biophys. Acta, Bioenerg.* **449**, 136-153.

15. Mathis, P., W. L. Butler and K. Satoh (1979) Carotenoid triplet state and chlorophyll fluorescence quenching in chloroplasts and subchloroplast particles. *Photochem. Photobiol.* **30**, 603-614.

16. Angerhofer, A., F. Bornhauser, A. Gall and R. J. Cogdell (1995) Optical and optically detected magnetic-resonance investigation on purple photosynthetic bacterial antenna complexes. *Chem. Phys.* **194**, 259-274.

17. Bonetti, C., M. T. A. Alexandre, R. G. Hiller, J. T. M. Kennis and R. van Grondelle (2009) Chl-a triplet quenching by peridinin in H-PCP and organic solvent revealed by step-scan FTIR time-resolved spectroscopy. *Chem. Phys.* **357** 63-69.

18. Papagiannakis, E., I. H. M. van Stokkum, H. Fey, C. Büchel and R. van Grondelle (2005) Spectroscopic characterization of the excitation energy transfer in the fucoxanthin–chlorophyll protein of diatoms. *Photosynth. Res.* **86**, 241-250.

19. Khoroshyy, P., D. Bína, Z. Gardian, R. Litvín, J. Alster and J. Pšenčík (2018) Quenching of chlorophyll triplet states by carotenoids in algal light-harvesting complexes related to fucoxanthin-chlorophyll protein. *Photosynth. Res.* **135**, 213-225.

20. Ho, J., E. Kish, D. D. Mendez-Hernandez, K. WongCarter, S. Pillai, G. Kodis, J. Niklas, O. G. Poluektov, D. Gust, T. A. Moore, A. L. Moore, V. S. Batista and B. Robert (2017) Triplet-triplet energy transfer in artificial and natural photosynthetic antennas. *Proc. Natl. Acad. Sci. U. S. A.* **114**, E5513-E5521.

21. Gust, D., T. A. Moore and A. L. Moore (2009) Solar fuels via artificial photosynthesis. *Acc. Chem. Res.* **42**, 1890-1898.

22. Gust, D., T. A. Moore and A. L. Moore (2012) Realizing artificial photosynthesis. *Faraday Discuss.* **155**, 9-26.

23. WongCarter, K., M. J. Llansola-Portolés, G. Kodis, D. Gust, A. L. Moore and T. A. Moore (2018) Light harvesting, photoregulation, and photoprotection in selected artificial photosynthetic systems. In *Light harvesting in photosynthesis*. (Edited by R. v. G. R. Croce, H. van Amerongen and I. van Stokkum). CRC Press. Taylor and Francis Group Boca Raton, Florida.

24. Liao, P.-N., S. Pillai, D. Gust, T. A. Moore, A. L. Moore and P. J. Walla (2011) Two-photon study on the electronic interactions between the first excited singlet states in carotenoid−tetrapyrrole dyads. *J. Phys. Chem. A* **115**, 4082-4091.

25. Robinson, G. W. and R. P. Frosch (1963) Electronic excitation transfer and relaxation. *J. Chem. Phys.* **38**, 1187-1203.

26. van Stokkum, I. H. M., D. S. Larsen and R. van Grondelle (2004) Global and target analysis of time-resolved spectra. *Biochim. Biophys. Acta, Bioenerg.* **1657**, 82-104.

27. Cardoso, S. L., D. E. Nicodem, T. A. Moore, A. L. Moore and D. Gust (1996) Synthesis and fluorescence quenching studies of a series of carotenoporphyrins with carotenoids of various lenghts. *J. Braz. Chem. Soc* **7**, 19-30.

28. Fungo, F., L. Otero, E. Durantini, W. J. Thompson, J. J. Silber, T. A. Moore, A. L. Moore, D. Gust and L. Sereno (2003) Correlation of fluorescence quenching in carotenoporphyrin dyads with the energy of intramolecular charge transfer states. Effect of the number of conjugated double bonds of the carotenoid moiety. *Phys. Chem. Chem. Phys.* **5**, 469-475.

29. Frisch, M. J., G. W. Trucks, H. B. Schlegel, G. E. Scuseria, M. A. Robb, J. R. Cheeseman, G. Scalmani, V. Barone, B. Mennucci, G. A. Petersson, H. Nakatsuji, M. Caricato, X. Li, H. P. Hratchian, A. F. Izmaylov, J. Bloino, G. Zheng, J. L. Sonnenberg, M. Hada, M. Ehara, K. Toyota, R. Fukuda, J. Hasegawa, M. Ishida, T. Nakajima, Y. Honda, O. Kitao, H. Nakai, T. Vreven, J. A. Montgomery Jr., J. E. Peralta, F. Ogliaro, M. J. Bearpark, J. Heyd, E. N. Brothers, K. N. Kudin, V. N. Staroverov, R. Kobayashi, J. Normand, K. Raghavachari, A. P. Rendell, J. C. Burant, S. S. Iyengar, J. Tomasi, M. Cossi, N. Rega, N. J. Millam, M. Klene, J. E. Knox, J. B. Cross, V. Bakken, C. Adamo, J. Jaramillo, R. Gomperts, R. E. Stratmann, O. Yazyev, A. J. Austin, R. Cammi, C. Pomelli, J. W. Ochterski, R. L. Martin, K. Morokuma, V. G. Zakrzewski, G. A. Voth, P. Salvador, J. J. Dannenberg, S. Dapprich, A. D. Daniels, Ö. Farkas, J. B. Foresman, J. V. Ortiz, J. Cioslowski and D. J. Fox (2009) Gaussian 09. Gaussian, Inc., Wallingford, CT, USA.

30. Shao, Y., L. F. Molnar, Y. Jung, J. Kussmann, C. Ochsenfeld, S. T. Brown, A. T. B. Gilbert, L. V. Slipchenko, S. V. Levchenko, D. P. O'Neill, R. A. DiStasio Jr., R. C. Lochan, T.

Wang, G. J. O. Beran, N. A. Besley, J. M. Herbert, C. Y. Lin, T. Van Voorhis, S. H. Chien, A. Sodt, R. P. Steele, V. A. Rassolov, P. E. Maslen, P. P. Korambath, R. D. Adamson, B. Austin, J. Baker, E. F. C. Byrd, H. Dachsel, R. J. Doerksen, A. Dreuw, B. D. Dunietz, A. D. Dutoi, T. R. Furlani, S. R. Gwaltney, A. Heyden, S. Hirata, C.-P. Hsu, G. Kedziora, R. Z. Khalliulin, P. Klunzinger, A. M. Lee, M. S. Lee, W. Liang, I. Lotan, N. Nair, B. Peters, E. I. Proynov, P. A. Pieniazek, Y. M. Rhee, J. Ritchie, E. Rosta, C. D. Sherrill, A. C. Simmonett, J. E. Subotnik, H. L. Woodcock III, W. Zhang, A. T. Bell, A. K. Chakraborty, D. M. Chipman, F. J. Keil, A. Warshel, W. J. Hehre, H. F. Schaefer III, J. Kong, A. I. Krylov, P. M. W. Gill and M. Head-Gordon (2006) Advances in methods and algorithms in a modern quantum chemistry program package. *Phys. Chem. Chem. Phys.* **8**, 3172-3191.

31. Becke, A. D. (1993) Density-functional thermochemistry. Iii. The role of exact exchange. *J. Chem. Phys.* **98**, 5648-5652.

32. Grimme, S., S. Ehrlich and L. Goerigk (2011) Effect of the damping function in dispersion corrected density functional theory. *J. Comput. Chem.* **32**, 1456-1465.

33. Hsu, C. P., Z. Q. You and H. C. Chen (2008) Characterization of the short-range couplings in excitation energy transfer. *J. Phys. Chem. C* **112**, 1204-1212.

34. You, Z.-Q. and C.-P. Hsu (2014) Theory and calculation for the electronic coupling in excitation energy transfer. *Int. J. Quantum Chem.* **114**, 102–115.

35. Arellano, J. B., T. B. Melo, P. K. Fyfe, R. J. Cogdell and K. R. Naqvi (2004) Multichannel flash spectroscopy of the reaction centers of wild-type and mutant *rhodobacter*

sphaeroides: Bacteriochlorophyllb-mediated interaction between the carotenoid triplet and the special pair. *Photochem. Photobiol.* **79**, 68-75.

36. Mandal, S., A.-M. Anne-Marie Carey, J. Locsin, B.-R. Gao, J. C. Williams, J. P. Allen, S. Lin and N. W. Woodbury (2017) Mechanism of triplet energy transfer in photosynthetic bacterial reaction centers. *J. Phys. Chem. B* **121**, 6499-6510.

37. You, Z.-Q. and C.-P. Hsu (2010) The fragment spin difference scheme for triplet-triplet energy transfer coupling. *J. Chem. Phys.* **133**, 074105.

38. Fiedor, L. and M. Pilch (2018) Side methyl groups control the conformation and contribute to symmetry breaking of isoprenoid chromophores. *Angew. Chem., Int. Ed. Engl.* **57**, 6501-6506.

39. Voet, D., J. G. Voet and C. W. Pratt (2016) *Fundamentals of biochemistry, life at the molecular level.* John Wiley and Sons, Singapore.

Table 1. Computed T-T energy transfer coupling for model dyads (in cm^{-1}).

Compound	V (cm^{-1})
Dyad-9'	11.5
Dyad-10'	13.7
Dyad-11'	8.7
Dyad-9''	19.4 (11.6)[a]
Dyad-10''	17.8 (17.5)[a]
Dyad-11''	16.5 (15.1)[a]
Dyad-9'''	16.9
Dyad-10'	13.7
Dyad-11'''	12.6

[a] Model dyads with their carotenoid constrained to curved conformation in dyads-9', 10' and 11', respectively.

FIGURES

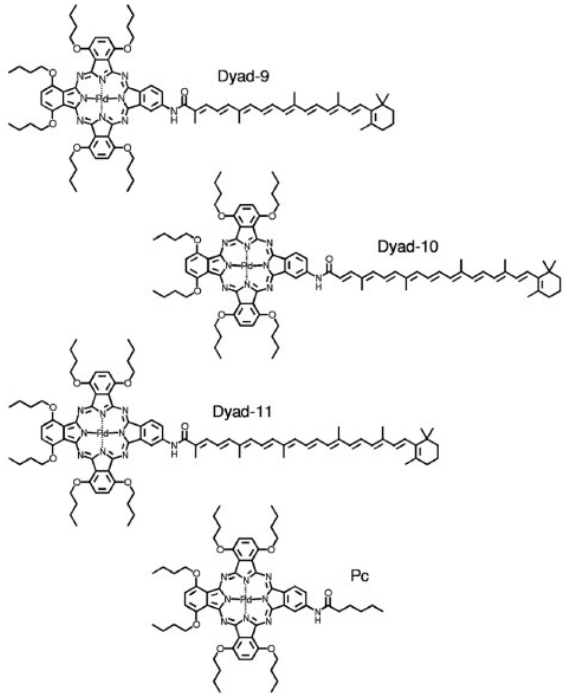

Figure 1. Molecular structures of the phthalocyanine reference (**Pc**) and carotenophthalocyanine dyads with 9, 10, and 11 conjugated double bonds.

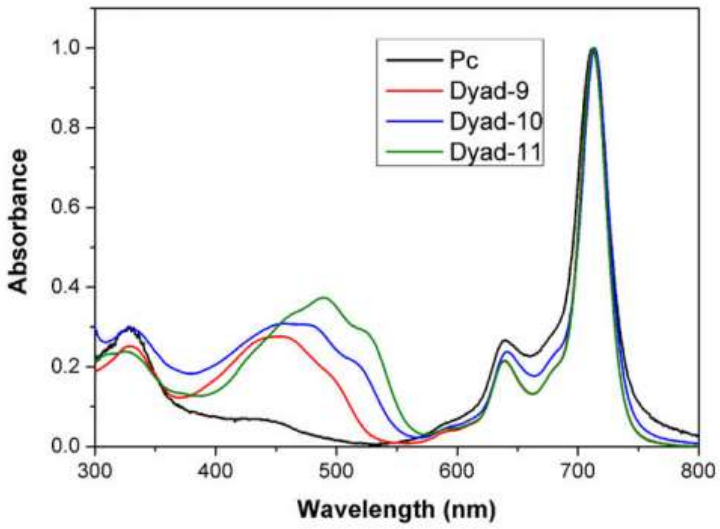

564

565 **Figure 2.** Absorption spectra in toluene of **dyad-9**, **dyad-10**, **dyad-11**, and **Pc** (black).

566

567

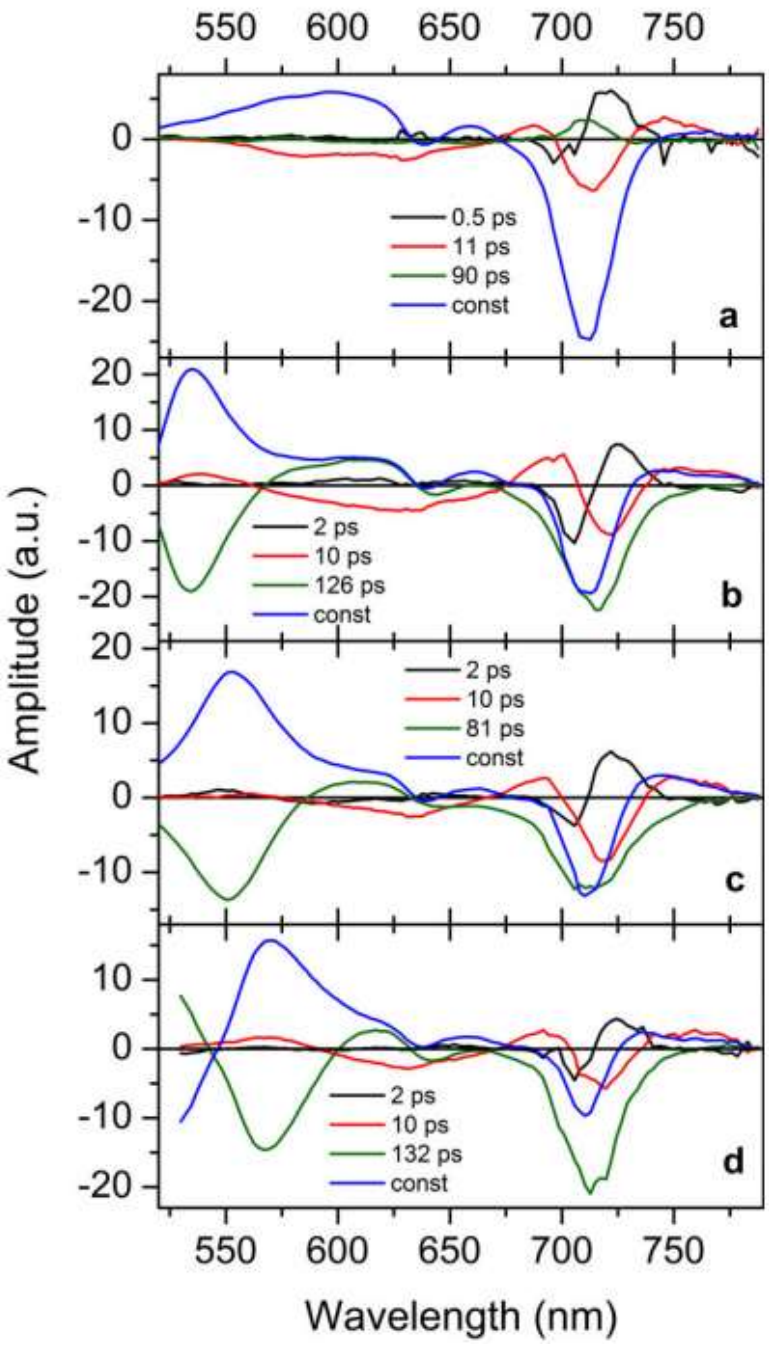

Figure 3. Decay-associated-spectra in toluene of **Pc** (a), **dyad-9** (b), **dyad-10** (c), and **dyad-11** (d) obtained from the transient absorption data upon excitation at 700 nm. On the 1 ns time window the ^{3}**Pc** and ^{3}carotenoid transient triplet species (^{3}**Car**) of the dyads do not decay and are shown as constants.

573

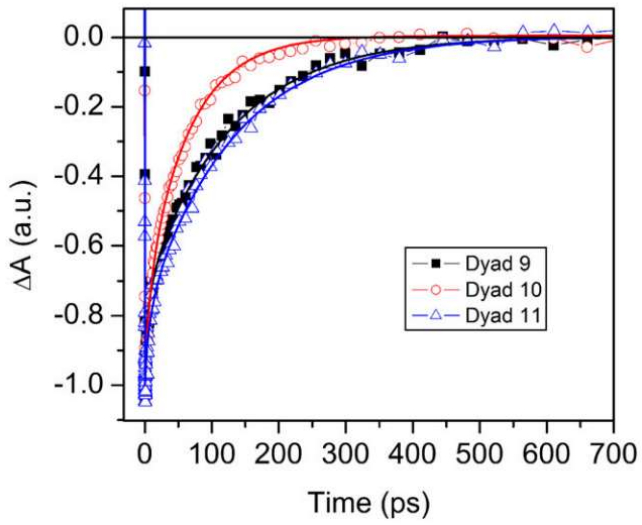

574

575 **Figure 4.** Decay kinetics and exponential fit (lines) at 710 nm for **dyad-9** (squares), **dyad-10**
576 (circles) and **dyad-11** (triangles) showing the transient absorption decay due to the T-T energy
577 transfer from ^{3}**Pc** to ^{3}**Car**. The decay kinetics has been normalized after the constant component
578 subtraction.

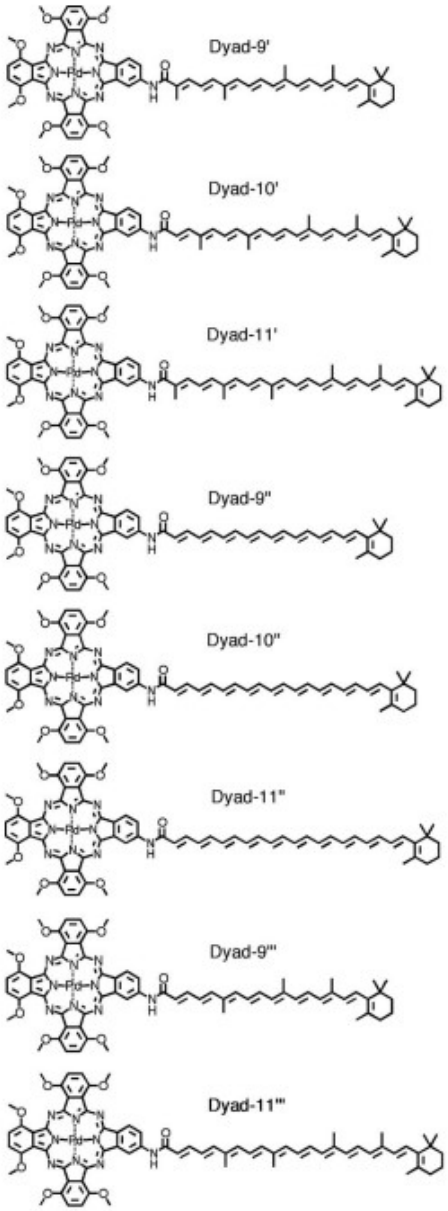

579

580 **Figure 5.** Computational models used in the determination of the T-T energy transfer coupling

581 (see Table 1).

582

583

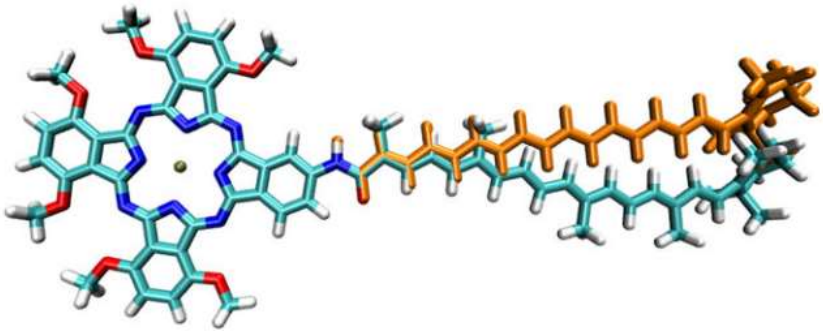

Figure 6. The conformation of the carotenoid in the DFT optimized geometries of **dyad-9'** and **dyad-9''** (orange).